# Nanoscale

Accepted Manuscript


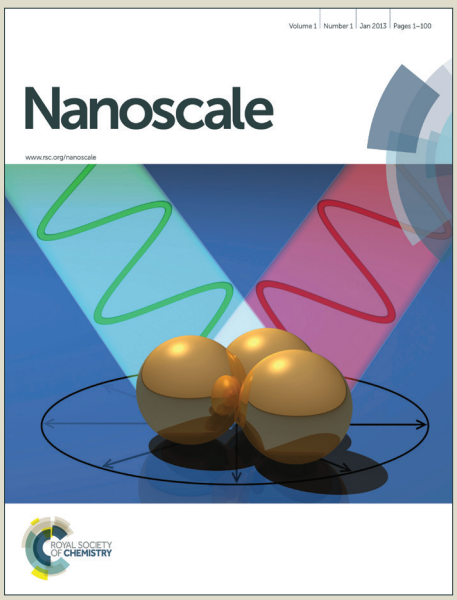





ROYAL SOCIETY OF CHEMISTRY

www.rsc.org/nanoscale

# Real-time, non-invasive monitoring of hydrogel degradation using $LiYF_4:Yb^{3+}/Tm^{3+}$ NIR-to-NIR upconverting nanoparticles

Ghulam Jalani[a], Rafik Naccache[b], Derek H Rosenzweig[c], Sophie Lerouge[d], Lisbet Haglund[c], Fiorenzo Vetrone[b]* and Marta Cerruti[a]*

[a]Department of Mining and Materials Engineering, McGill University, Montreal, QC, H3A 0C5, Canada

[b]Institut National de la Recherche Scientifique-Énergie, Matériaux et Télécommunications, Université du Québec, Varennes, QC, J3X 1S2, Canada

[c]Department of Surgery, McGill University, Montreal, QC, H3G 1A4, Canada

[d]Department of Mechanical Engineering, École de technologie supérieure & Centre de recherche du CHUM (CRCHUM), Montreal, QC, H3C 1K3, Canada

**Keywords.** Non-invasive, upconverting nanoparticles, hydrogels, degradation

**Abstract**

To design a biodegradable hydrogel as cell support, one should know its *in-vivo* degradation rate. A technique commonly used to track gel degradation is fluorescence spectroscopy. However, the fluorescence from conventional fluorophores quickly decays, and the fluorophores are often moderately cytotoxic. Most importantly, they require ultraviolet or visible (UV-Vis) light as the excitation source, which cannot penetrate deeply through biological tissues. Lanthanide-doped upconverting nanoparticles (UCNPs) are exciting alternatives to conventional fluorophores because they can convert near-infrared (NIR) to UV-Vis-NIR light via a sequential multiphoton absorption process referred to as upconversion. NIR light can penetrate up to few cm inside tissues, thus making these UCNPs much better probes than conventional fluorophores for *in-vivo* monitoring. Also, UCNPs have narrow emission bands, high photoluminescence (PL) signal-to-noise ratio, low cytotoxicity and good physical and chemical stability. Here, we show a nanocomposite system consisting of a biodegradable, *in-situ* thermogelling injectable hydrogel made of chitosan and hyaluronic acid encapsulating silica-coated $LiYF_4:Yb^{3+}/Tm^{3+}$ UCNPs. We use these UCNPs as photoluminescent tags to monitor the gel degradation inside live, cultured intervertebral discs (IVDs) over a period of 3 weeks. PL spectroscopy and NIR imaging show that NIR-to-NIR upconversion of $LiYF_4:Yb^{3+}/Tm^{3+}@SiO_2$ UCNPs allows for tracking of the gel degradation in living tissues. Both *in-vitro* and *ex-vivo* release of UCNPs follow a similar trend during the first 5 days; after this time, *ex-vivo* release becomes faster than *in-vitro*, indicating a faster gel degradation *ex-vivo*. Also, the amount of released UCNPs *in-vitro* increases continuously up to 3 weeks, while it plateaus after 15 days inside the IVDs showing a homogenous distribution of UCNPs throughout the IVD tissue. This non-invasive optical method

for real time, live tissue imaging holds great potential for tissue analysis, biomapping and bioimaging applications.

## Introduction

Biodegradable hydrogels are three dimensional (3D) crosslinked polymeric networks widely used as cell supports in tissue engineering. Their main functions include providing mechanical support and a physiological environment where cells can thrive.[1] The hydrogels degrade over time and are eventually replaced by newly formed tissue.[2] The gel degradation rate should closely match the secretion rate of newly formed extracellular matrix (ECM) by the encapsulated cells. If the gel degrades too quickly, it will not be able to hold the cells and may expose them to external forces; also, it will not be able to retain ECM components, resulting in premature tissue degeneration. On the other hand, if the degradation is too slow, ECM components can accumulate at pericellular regions causing cellular stress, altered cellular functions or even cell death.[3] Hydrogel degradation monitoring is thus crucial to design a suitable scaffold. It is, however, quite challenging to track hydrogel degradation *in-vivo*. Strategies developed for *in-vitro* degradation monitoring include bulk weight loss measurement,[4] multiple particle tracking rheometry[5] and chromatography.[6] None of these methods can be applied to real-time monitoring *in-vivo* since they require the gel to be placed in a dedicated instrument. If they are used to test gel degradation upon removal from the body, they require a large number of animals and involve multiple surgeries, giving rise to variable results.[7]

The principal methods explored to date for real-time *in-vivo* gel degradation monitoring are magnetic resonance imaging (MRI) and fluorescence spectroscopy. MRI is attractive because of

its high spatial resolution, but it requires magnetically active materials as contrast agents and sophisticated instrumentation.[8] Fluorescence-based assays therefore remain the most widely used method for hydrogel tracking *in-vivo*. For example, recently, Artzi et al. fluorescently labeled polyethylene glycol (PEG) hydrogels to track their degradation *in-vivo* and developed a correlation with *in-vitro* degradation.[9] Ong et al. used an epitope as a labelling agent to monitor the degradation of elastin-like polypeptide gels through enzyme-linked immunosorbent assay.[10] The amount of leached-out antibodies was considered as a measure of gel degradation. Similarly, porphyrin-based crosslinkers and rhodamine B-based fluorescent dyes have been used to locate the gel implants and monitor degradation rate in-vivo.[11, 12] Fluorescence-based assays are simple and inexpensive but have some serious drawbacks when used in biological systems. Most of the fluorescent labels consist of organic dyes, which have poor photostability[13] and are prone to photobleaching during long exposures to lasers. Moreover, the dyes are often chemically conjugated to the hydrogels to prevent their release through diffusion; this can affect gel degradation.[14] Finally, most of the fluorescent tags require UV or visible excitation. UV light is carcinogenic, and a prolonged exposure can be harmful to the tissues.[15] Both UV and visible light frequencies are largely absorbed by biomolecules already present in the tissues, resulting in low signal outputs.[16, 17]

An approach based on NIR radiation can be used to address the latter crucial point. NIR can penetrate up to few cm beneath the skin, since in the wavelength region of 650 - 1350 nm, scattering dominates rather than absorption in biological tissues.[18] Also, NIR excitation does not impart background fluorescence from biomolecules, resulting in higher detection sensitivity. A few NIR-excitable fluorophores have been developed, which show deeper penetration compared to UV-Vis excitable fluorophores, minimal autofluorescence and high signal-to-noise ratios.[19, 20]

Most of these fluorophores, however, are comprised of organic molecules (dyes) which lack the required photostability and cytocompatibility.[21]

Lanthanide-doped UCNPs have emerged as alternatives to these NIR-excitable fluorophores (*e.g.* organic dyes and semiconductor quantum dots).[22] This stems primarily from their photophysical properties brought about by the intra 4*f* transitions of the lanthanide dopants.[23] Many of the lanthanide ions possess multiple 4*f* electronic energy states with long lifetimes allowing them to act as population reservoirs in the upconversion process.[24] Hence, the use of costly femtosecond excitation sources is not required as the multiphoton process occurs through a sequential, ladder-like addition of NIR photons (typically 980 nm).[25] In particular, certain $Ln^{3+}$ ions (such as $Tm^{3+}$) can upconvert the 980 nm excitation light to higher energies, yet still in the NIR region (800 nm) *via* a two-photon process.[26, 27] In this case, both the excitation and emission wavelengths lie within the first biological window making them ideal for a slew of biological applications, especially *in vivo* imaging.[28-30] Upconversion has been reported in various nanoscale hosts including oxides, vanadates, phosphates and fluorides to name a few.[31, 32] The latter are ideal for doping with lanthanide ions due to their low vibrational (phonon) energies, excellent physical and photochemical stability, but most importantly for biological applications due to their low cytotoxicity.[33] For $Tm^{3+}$-doping, $LiYF_4$ has been shown to be particularly adept as a host. When excited at 980 nm, $LiYF_4$:$Yb^{3+}$/$Tm^{3+}$ UCNPs ($Yb^{3+}$ ions are used as the sensitizers in the upconversion process[23]) exhibits intense upconverted luminescence spanning the UV, visible, and NIR regions.[34, 35]

Here we show silica-coated $LiYF_4:Yb^{3+}/Tm^{3+}$ UCNPs (UCNPs@$SiO_2$) as NIR-excited photoluminescent nano-trackers for non-invasive monitoring of hydrogel degradation. We select these particles because $Tm^{3+}$ doping results in NIR upconverted emission in addition to visible and UV emissions, thus allowing these particles to be both excited and monitored through biological tissues. Hence, both excitation and emission wavelengths lie within the tissue penetration window. We coat the UCNPs with $SiO_2$ (UCNPs@$SiO_2$) to make their surfaces hydrophilic and then homogeneously disperse them in chitosan-hyaluronic acid (CH-HA) mixtures that can gel upon crosslinking with β-glycerophosphate (BGP) and genipin (GN). While the mixtures are still soft, we inject them into the central nucleus pulposus of *ex-vivo* cultured intervertebral discs (IVDs),[36] which provide an excellent platform for simulating the *in-vivo* environment since they can be kept alive for several weeks. After injecting the UCNPs@$SiO_2$–loaded gels approximately 6 mm below the disc surface, we use a 975 nm laser to excite the $Yb^{3+}$ dopant in the $LiYF_4:Yb^{3+}/Tm^{3+}$ UCNPs, and record their upconverted emission at 792 nm from the $^1G_4 \rightarrow {}^3H_5$ and $^3H_4 \rightarrow {}^3H_6$ transitions of the $Tm^{3+}$ ion[34, 37] using a spectrophotometer and a NIR camera. Using this simple setup, we are able to spatially localize the UCNPs throughout the IVD over a period of three weeks, thus monitoring gel degradation in real time. *Ex-vivo* results closely match *in-vitro* experiments, showing that the UCNPs stay well encapsulated inside the gel and do not diffuse without gel degradation. An equilibrium is established *ex-vivo* after approximately 2 weeks; following this period, the UCNPs are homogeneously dispersed inside the IVDs, since they cannot easily diffuse outside them. These results show that Tm-doped NIR-to-NIR UCNPs@$SiO_2$ can be used for relatively deep[26] and sensitive non-invasive tracking of hydrogel degradation inside living tissues over long periods of time.

**Results and discussion**

Figure 1 shows the schematics of our experimental design. We have previously shown that highly homogenous, thermogelling, injectable gels can be prepared from CH and HA at physiological pH using both BGP and GN as co-crosslinkers.[38] Here we encapsulate $LiYF_4:Yb^{3+}/Tm^{3+}$ coated with silica (UCNPs@$SiO_2$) in these gels and use them to monitor the gel degradation in live IVDs. To prepare hydrogels embedded with UCNPs, we first prepare an acidic solution of CH at pH 6.2. We then add BGP to simultaneously neutralize the charge of CH and raise its pH to 7.25 (A), and then mix in the HA, GN and UCNPs@$SiO_2$ solutions (B). Subsequently, this mixture is injected into the pre-trypsinized nucleus pulposus tissues of IVDs (C). Trypsin partially degrades the nucleus pulposus, inducing a degenerate-like environment and facilitates hydrogel injections.[36] We then immerse the IVDs in Dulbecco's Modified Eagle's Medium-High Glucose (DMEM-HG) growth medium and raise the temperature to 37 ºC in a standard cell culture incubator, to convert the solutions to gels (D). The IVDs are irradiated with a 975 nm diode laser after 3, 5, 8, 15 and 22 days of culture. The UCNPs@$SiO_2$ encapsulated inside the gel upconvert the low energy NIR incident light at 975 nm to higher energy NIR light at 792 nm via an energy transfer process from two excited $Yb^{3+}$ ions in close proximity to a single $Tm^{3+}$ ion (a two-photon process).[34] The upconverted NIR light at 792 nm is then captured using a NIR camera equipped with appropriate filters (E and F). The upconversion PL spectra of UCNPs@$SiO_2$ are subsequently recorded using a fiber-coupled spectrophotometer (G).

We synthesized highly homogenous $LiYF_4:Yb^{3+}/Tm^{3+}$ UCNPs via the thermal decomposition of trifluoroacetates of Li, Y, Yb and Tm in the presence of 1-octadecene (OD) and oleic acid

(OA).[34, 39] The resulting UCNPs are capped with a layer of OA molecules, which ensures their dispersion in non-polar solvents such as hexane. The TEM image in Figure 2A shows that highly monodispersed diamond-shaped UCNPs with narrow size distribution are obtained. The average length, width and thickness of the UCNPs are 78 ± 9nm, 43 ± 6nm and 8 ± 1nm, respectively. This is in accordance with our previously reported results[34] that thermal decomposition is an efficient method to synthesize high quality UCNPs with narrow size distribution. The resulting UCNPs are readily dispersed in organic solvents. However, to allow for integration in biological applications, the UCNPs should be dispersed in water or other hydrophilic media. We convert the OA-capped hydrophobic UCNPs to hydrophilic UCNPs by coating them with a thin shell of silica ($SiO_2$) using a reverse micro-emulsion process. TEM images reveal that an 8 ± 2 nm thick shell of $SiO_2$ is obtained around each UCNP (Figure 2B). Moreover, all UCNPs are individually coated and do not aggregate during the formation of the silica shell.

To evaluate PL properties of the UCNPs we record the upconversion emission spectra of UCNPs and UCNPs@$SiO_2$. Excitation of a 1% (w/v) suspension of UCNPs (in hexane) and UCNPs@$SiO_2$ (in DI water) by a 975 nm laser shows strong emissions spanning the UV, Vis and NIR regions (Figure 2C). The upconverted PL spectrum of the UCNPs shows two UV emission bands at 347 and 362 nm corresponding to the $^3P_0 \rightarrow {}^3F_4$ and $^1D_2 \rightarrow {}^3H_6$ transitions; four visible bands at 449, 483, 512 and 649 nm, corresponding to the $^1D_2 \rightarrow {}^3F_4$, $^1G_4 \rightarrow {}^3H_6$, $^1D_2 \rightarrow {}^3H_5$ and $^1G_4 \rightarrow {}^3F_4$ transitions; and a strong NIR peak at 792 nm, which can be attributed to the $^1G_4 \rightarrow {}^3H_5$ and $^3H_4 \rightarrow {}^3H_6$ transition.[34, 37] The PL spectrum of UCNPs@$SiO_2$ shows similar but less intense emission bands. The lower intensity is most likely due to quenching due to the silica shell

resulting from the large phonon energies of the $SiO_2$ matrix. X-ray diffraction (XRD) shows that both UCNPs and UCNPs@$SiO_2$ are crystalline, with tetragonal crystal structure matching the one expected for $LiYF_4$ (Figures 2D and S1).

We evaluate the cytotoxicity of UCNPs@$SiO_2$ by culturing isolated primary chondrocyte[37] cells in DMEM-HG supplemented with UCNPs@$SiO_2$ in concentrations ranging from 0.05-0.5mg/ml. Live/dead fluorescence images (Figure 2E-2G) show that more than 95% of cells are viable after 48 h of culture in all samples, which confirms the excellent biocompatibility of UCNPs@$SiO_2$.

To study the effect of UCNPs@$SiO_2$ on the mechanical properties of gels, we compared the behavior in compression of CH-HA-BGP-GN/UCNPs@$SiO_2$ and CH-HA-BGP-GN gels (see table S1) using unconfined compression testing at a constant strain rate of 1.66%/sec. We also prepared control samples crosslinked with either BGP or GN. As shown by stress-strain curves (Figure 3A), all gels sustain up to 50% deformation, and the addition of UCNPs did not affect the non-linear behavior in compression, except at high strain (above 40%) where higher rigidity is observed. The compressive stress at 50% strain increases in the order CH-HA-BGP (7.9 kPa) < CH-HA-GN (18.9 kPa) < CH-HA-BGP-GN (22.1 kPa) < CH-HA-BGP-GN/UCNPs@$SiO_2$ (31.8 kPa). Stress-strain curves obtained during compression and recovery show that all gels exhibit complete structure restoration, which confirms their excellent elastic properties (Figure S2). These results agree with our previous findings indicating that co-crosslinking significantly improves gel strength,[38] and suggest that the addition of UCNPs@$SiO_2$ further improves the

compressive strength of CH-HA gels. This is likely due to the higher resistance to deformation offered by the inorganic UCNPs embedded inside the hydrogel matrix.[40]

To evaluate UCNPs release from the gels *in-vitro*, we immerse freeze dried CH-HA-BGP-GN/UCNPs@$SiO_2$ scaffolds in PBS and PBS with the addition of lysozyme (PBS-Lys) over three weeks, and recorded the gel weight-loss (Figure 3B) and amount of released UCNPs (Figure 3C) at regular intervals. Almost no degradation is observed during the first 3 days (Figure 3B). After one week of incubation in PBS-Lys, the gels lose approximately 15% of their initial weight, and ~85% after 3 weeks. Somewhat lower values (on average ~17%) are measured in PBS alone. UCNP release (Figure 3C) follows a very similar trend: no UCNPs are detected during the first three days; ~12% of the UCNPs initially loaded are released after one week of incubation in PBS-Lys, and this value reaches ~80% after 3 weeks. Again, ~19% lower values are found in PBS alone. These matching trends suggest that UCNP-release can be used as an indication of hydrogel degradation.

To confirm this, we fit the UCNP release using the Ritger and Peppas model.[41] This model was originally developed to describe the release of solutes from polymeric materials (e.g. hydroxypropyl methyl cellulose, poly (vinyl alcohol), poly (2-hydroxyethyl-methacrylate etc.) According to this model, the release at any given time ($M_t$) can be described by

$$M_t/M_\infty = kt^n \qquad \text{(Equation 1)}$$

where $M_\infty$ is the concentration at equilibrium (total amount of UCNPs loaded in the hydrogel), $k$ is a constant related to the polymeric structure where the UCNPs are encapsulated, $t$ is time and $n$ relates to the mechanism of UCNP release. Using Equation 1 to fit the curves shown in Figure 3C, we calculate values for $n$ of 0.53 ($R^2$=0.99) and 0.58 ($R^2$= 0.98) for degradation in PBS and PBS-Lys respectively. Values of $n$ between 0.45 and 1.0 correspond to non-Fickian diffusion,[41] which confirms that UCNP release is not controlled by diffusion alone, but has to be related to gel degradation too.

To test the applicability of UCNPs@$SiO_2$ in *ex-vivo* real time gel degradation monitoring, we inject 150 µl of a CH-HA-BGP-GN/UCNPs@$SiO_2$ mixture into pre-trypsinized nucleus pulposus tissue of a live IVD. We prepare two IVDs; one for "day zero" and the other for the rest of the experiment. The average diameter and thickness of the IVDs are 26 ± 2 and 11 ± 1 mm, respectively. We position a NIR camera on one side of the IVD, with a band-pass filter in front of it, to only allow for the collection of the NIR light emitted by the UCNPs. We use this setup to capture images through the whole IVD thickness while shining an unfocused 975 nm laser light on the IVD at the locations schematically shown in Figure 4A. The NIR images collected following laser excitation from the top of the IVD (Figure 4B-P1) at different spots on day zero (Figure 4C), show emitted radiation only in the image collected at the center of the IVD (spot O), corresponding to the injection site. The image collected in spot O shows a bright spot at the top (Figure 4C-P1-O), and light emitted throughout the whole disk. This proves several points: (i) UCNPs are efficiently excited throughout the whole vertical section of the disc (labeled as "t" in Figure 4A); (ii) the upconverted light travels a distance of ~1.2 cm (the radius of IVD, labeled as "r" in Figure 4A), since it can be captured by the NIR camera positioned outside the disc; and

(iii) at day zero, all UCNPs are localized at the injection site. To clarify the origin of the brighter spot seen in Figure 4C-P1-O, we capture similar images in a reversed configuration (Figure 4B-P2), i.e. illuminating with the laser from the bottom of the IVD. Also in this configuration, UCNPs are observed only at the central location (spot O); however, in this case, the brighter spot is seen at the bottom of the image (Figure 4C-P2-O). This implies that the bright spot seen at the disk surface is not related to a high UCNP concentration in this location, but rather to higher laser intensity.

The images captured while the laser illuminated the top of the IVD on different locations on day 3, 5, 8, 15 and 22 are shown in figure 5A. After 3 days, all of the UCNPs are still located at the center of the IVD (spot O), thus indicating that no degradation is occurring, and the UCNPs are not diffusing out of the gel. This result correlates well with the *in-vitro* UCNP release and gel degradation results (Figures 3B and 3C). After 5 days, a small amount of UCNPs is detected in points A and A'; however, most of the UCNPs are still visible at the center of the IVD. After one week of culture, a significant amount of UCNPs leave the gel and diffuse outwards, as shown by the increasing intensity of the NIR images taken at spots A, A', B and B'. At the same time, the central region of the IVD is continuously depleted of UCNPs, as indicated by the gradually decreasing intensity measured at point O. This phenomenon continues in the following week (see images collected after 15 days of culture). The images captured on day 22 are very similar to those captured after 15 days, thus showing that an equilibrium is reached.

We quantified these observations by plotting the total integrated intensity of the images as a function of time (Figure S4). The intensity at spot O continuously decreases during the first two weeks and then plateaus. An opposite trend is observed at spots A, A', B and B'.

The PL spectra emitted by the UCNPs@$SiO_2$ was recorded while the laser illuminated different spots and time points are shown in Figure S5, and in Figure 5B, we report the intensity of the band at 792 nm as a function of time at each spot. All other emission bands observed in the UV and Vis region (Figure 2C) are absorbed by the tissue (Figure S5A, spot O); only the NIR peak can penetrate the 1.2 cm-thick tissue of the IVD and be detected, thus underscoring the necessity of NIR-to-NIR upconversion for deep tissue imaging. For clarity, we have plotted only the 700-850 nm portion of the upconversion spectra on all other panels shown in Figure S5. The trends shown in Figure 5B closely match those measured from the NIR images (Figure S4): the signal emitted from the UCNPs present in spot O decreases during the first two weeks and almost plateaus at the third week, while the signals recorded from points A, A', B and B' follow an opposite trend.

The *in-vitro* UCNP release previously reported as a histogram in Figure 3C is also re-plotted in Figure 5B for comparison (dotted red line). The *in-vitro* UCNP release closely matches UCNP release inside the IVD during the first 5 days. After this time, UCNP release in the IVD is more rapid compared to the *in-vitro* one, thus indicating a faster gel degradation *ex-vivo*. The faster release of nanoparticles inside the IVD might be due to cell migration, cell growth or cell apoptosis inside the IVD. The *in-vitro* signal keeps increasing continuously up to 22 days, while

it plateaus after 15 days in the IVD. This difference can most likely be related to the limited diffusion of the UCNPs outside the IVD, while the gel containing the UCNPs is directly in contact with PBS *in-vitro*.

## Conclusions

In summary, this is the first report showing the use of UCNPs to track hydrogel degradation in live tissues; we achieved this by exploiting NIR-to-NIR upconversion, which allowed us to monitor the UCNP location in living tissues non-invasively. Unlike organic dyes, the UCNPs stay well encapsulated inside the gels, and do not significantly leach or diffuse outside in the absence of gel degradation. This eliminates the need for chemical conjugation to the gels, which introduces artifacts. The UCNPs are highly biocompatible and do not cause toxicity to the cells, while making the gels more resistant to deformation under compression. This highly versatile platform can be used to estimate the extent of degradation of biodegradable gels with high sensitivity *in-vivo*, for example in tissue regeneration and therapeutics delivery through degradable polymeric nanoparticles. Furthermore, *in-situ* generation of UV and Vis light can potentially be used for photo-triggered drug release from photodegradable hydrogels, making this system a multifunctional theranostic platform.

## Supplementary Information.

Electronic Supplementary Information (ESI) is available and includes additional XRD, compression testing, cell viability and PL spectroscopy results. See DOI: 10.1039/x0xx00000x

**Acknowledgments**

This work was supported by Natural Sciences and Engineering Research Council of Canada (NSERC), Fonds de recherche du Québec – Nature et technologies (FRQNT), Center for Self-assembled Chemical Structures (CSACS), Canada Research Chairs (CRC), Canada Foundation for Innovation (CFI) and McGill Engineering Doctoral Award (MEDA). We acknowledge Dr. Marta Quintanilla for helping with PL measurements, Ms. Janet Moir for discs preparation and Prof. Faleh Tamimi Marino for useful technical discussion.

**References**

1. J. M. Zhu and R. E. Marchant, *Expert Rev. Med. Devic.*, 2011, **8**, 607-626.
2. J. L. Drury and D. J. Mooney, *Biomaterials*, 2003, **24**, 4337-4351.
3. F. Guilak, L. G. Alexopoulos, M. L. Upton, I. Youn, J. B. Choi, L. Cao, L. A. Setton and M. A. Haider, *Ann. NY. Acad. Sci.*, 2006, **1068**, 498-512.
4. C. J. Bettinger, J. P. Bruggeman, J. T. Borenstein and R. S. Langer, *Biomaterials*, 2008, **29**, 2315-2325.
5. K. M. Schultz and K. S. Anseth, *Soft Matter*, 2013, **9**, 1570-1579.
6. C. Witt, K. Mader and T. Kissel, *Biomaterials*, 2000, **21**, 931-938.
7. O. Benny, S. K. Kim, K. Gvili, I. S. Radzishevsky, A. Mor, L. Verduzco, L. G. Menon, P. M. Black, M. Machluf and R. S. Carroll, *FASEB J.*, 2008, **22**, 488-499.
8. L. S. Karfeld, S. R. Bull, N. E. Davis, T. J. Meade and A. E. Barron, *Bioconjugate Chem.*, 2007, **18**, 1697-1700.
9. N. Artzi, N. Oliva, C. Puron, S. Shitreet, S. Artzi, A. bon Ramos, A. Groothuis, G. Sahagian and E. R. Edelman, *Nat. Mater.*, 2011, **10**, 704-709.
10. S. R. Ong, K. A. Trabbic-Carlson, D. L. Nettles, D. W. Lim, A. Chilkoti and L. A. Setton, *Biomaterials*, 2006, **27**, 1930-1935.
11. W. W. Wang, J. J. Liu, C. Li, J. Zhang, J. F. Liu, A. J. Dong and D. L. Kong, *J. Mater. Chem. B*, 2014, **2**, 4185-4192.
12. J. F. Lovell, A. Roxin, K. K. Ng, Q. C. Qi, J. D. McMullen, R. S. DaCosta and G. Zheng, *Biomacromolecules*, 2011, **12**, 3115-3118.
13. P. Sharma, S. Brown, G. Walter, S. Santra and B. Moudgil, *Adv. Colloid Interface Sci.*, 2006, **123-126**, 471-485.
14. A. Guan, Z. Li and K. S. Phillips, *J. Fluoresc.*, 2014, **24**, 1639-1650.
15. G. A. Wagnieres, W. M. Star and B. C. Wilson, *Photochem. Photobiol.*, 1998, **68**, 603-632.
16. S. L. Jacques, *Phys. Med. Biol.*, 2013, **58**, R37-61.

17. J. V. Frangioni, *Curr. Opin. Chem. Biol.*, 2003, **7**, 626-634.
18. R. Weissleder, *Nat. Biotechnol.*, 2001, **19**, 316-317.
19. G. S. Hong, J. C. Lee, J. T. Robinson, U. Raaz, L. M. Xie, N. F. Huang, J. P. Cooke and H. J. Dai, *Nat. Med.*, 2012, **18**, 1841-1846.
20. L. M. Maestro, J. E. Ramirez-Hernandez, N. Bogdan, J. A. Capobianco, F. Vetrone, J. G. Sole and D. Jaque, *Nanoscale*, 2012, **4**, 298-302.
21. I. L. Medintz, H. T. Uyeda, E. R. Goldman and H. Mattoussi, *Nat. Mater.*, 2005, **4**, 435-446.
22. S. Wilhelm, M. Kaiser, C. Wurth, J. Heiland, C. Carrillo-Carrion, V. Muhr, O. S. Wolfbeis, W. J. Parak, U. Resch-Genger and T. Hirsch, *Nanoscale*, 2015, **7**, 1403-1410.
23. F. Auzel, *Chem. Rev.*, 2004, **104**, 139-173.
24. M. Haase and H. Schafer, *Angew. Chem. Int. Edit.*, 2011, **50**, 5808-5829.
25. F. Wang and X. G. Liu, *Chem. Soc. Rev.*, 2009, **38**, 976-989.
26. G. Chen, J. Shen, T. Y. Ohulchanskyy, N. J. Patel, A. Kutikov, Z. Li, J. Song, R. K. Pandey, H. Ågren, P. N. Prasad and G. Han, *ACS Nano*, 2012, **6**, 8280-8287.
27. T. Passuello, M. Pedroni, F. Piccinelli, S. Polizzi, P. Marzola, S. Tambalo, G. Conti, D. Benati, F. Vetrone, M. Bettinelli and A. Speghini, *Nanoscale*, 2012, **4**, 7682-7689.
28. Q. Liu, Y. Sun, T. S. Yang, W. Feng, C. G. Li and F. Y. Li, *J. Am. Chem. Soc.*, 2011, **133**, 17122-17125.
29. Y. F. Wang, G. Y. Liu, L. D. Sun, J. W. Xiao, J. C. Zhou and C. H. Yan, *ACS Nano*, 2013, **7**, 7200-7206.
30. M. Nyk, R. Kumar, T. Y. Ohulchanskyy, E. J. Bergey and P. N. Prasad, *Nano Lett.*, 2008, **8**, 3834-3838.
31. E. Hemmer, F. Vetrone and K. Soga, *MRS Bull.*, 2014, **39**, 960-964.
32. J. Zhou, Q. Liu, W. Feng, Y. Sun and F. Y. Li, *Chem. Rev.*, 2015, **115**, 395-465.
33. F. Wang, D. Banerjee, Y. S. Liu, X. Y. Chen and X. G. Liu, *Analyst*, 2010, **135**, 1839-1854.
34. V. Mahalingam, F. Vetrone, R. Naccache, A. Speghini and J. A. Capobianco, *Adv. Mater.*, 2009, **21**, 4025-4028.
35. T. Cheng, R. F. Ortiz, K. Vedantham, R. Naccache, F. Vetrone, R. S. Marks and T. W. Steele, *Biomacromolecules*, 2015, **16**, 364-373.
36. R. Gawri, J. Moir, J. Ouellet, L. Beckman, T. Steffen, P. Roughley and L. Haglund, *PLoS One*, 2014, **9**, e101233.
37. M. Quintanilla, I. X. Cantarelli, M. Pedroni, A. Speghini and F. Vetrone, *J. Mater. Chem. C*, 2015, **3**, 3108-3113.
38. G. Jalani, D. H. Rosenzweig, G. Makhoul, S. Abdalla, R. Cecere, F. Vetrone, L. Haglund and M. Cerruti, *Macromol. Biosci.*, 2015, **15**, 473-480.
39. J. C. Boyer, F. Vetrone, L. A. Cuccia and J. A. Capobianco, *J. Am. Chem. Soc.*, 2006, **128**, 7444-7445.
40. J. L. Tsai and Y. L. Cheng, *J. Compos. Mater.*, 2009, **43**, 3143-3155.
41. P. L. Ritger and N. A. Peppas, *J. Controlled Release*, 1987, **5**, 23-36.

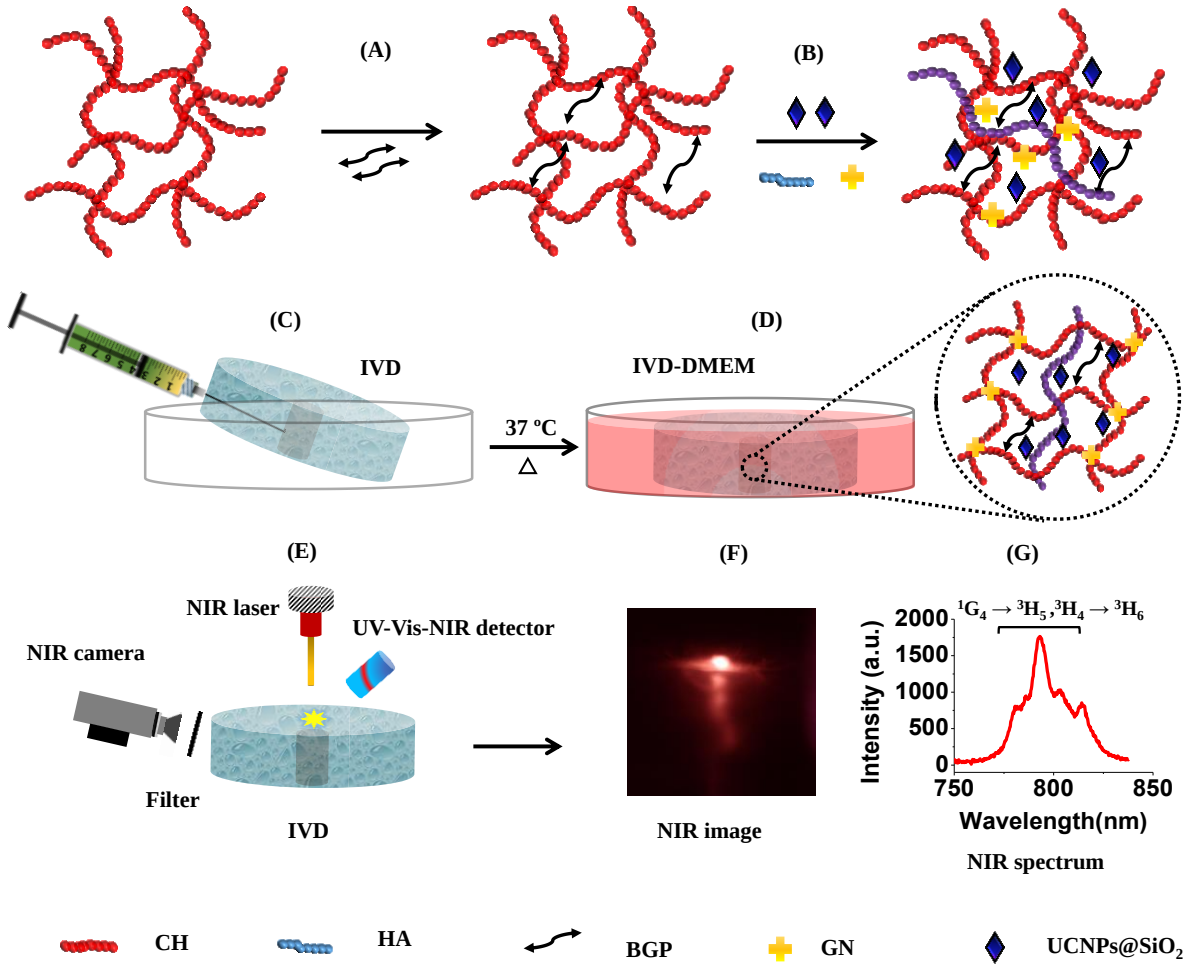


**Figure 1.** Schematic illustration of the synthesis of CH-HA-BGP-GN/UCNPs@$SiO_2$ composite gels, injection in IVD and NIR-mediated degradation tracking. All solutions are ice-cooled before mixing. An acidic solution of CH (pH = 6.2) is first neutralized by BGP to raise the pH to 7.25 (A), followed by the addition of HA, GN and UCNP@$SiO_2$ (B). The mixture is then injected into the nucleus pulposus region of IVDs (C). Then, the IVDs are immersed in DMEM-HG and incubated at 37 ºC in a cell culture incubator to produce composite gels *in-situ* (D). The IVDs are irradiated with a NIR laser (λ = 975 nm) and the upconverted emission at 792 nm is detected by a NIR camera and a fiber-coupled spectrophotometer (E-G).

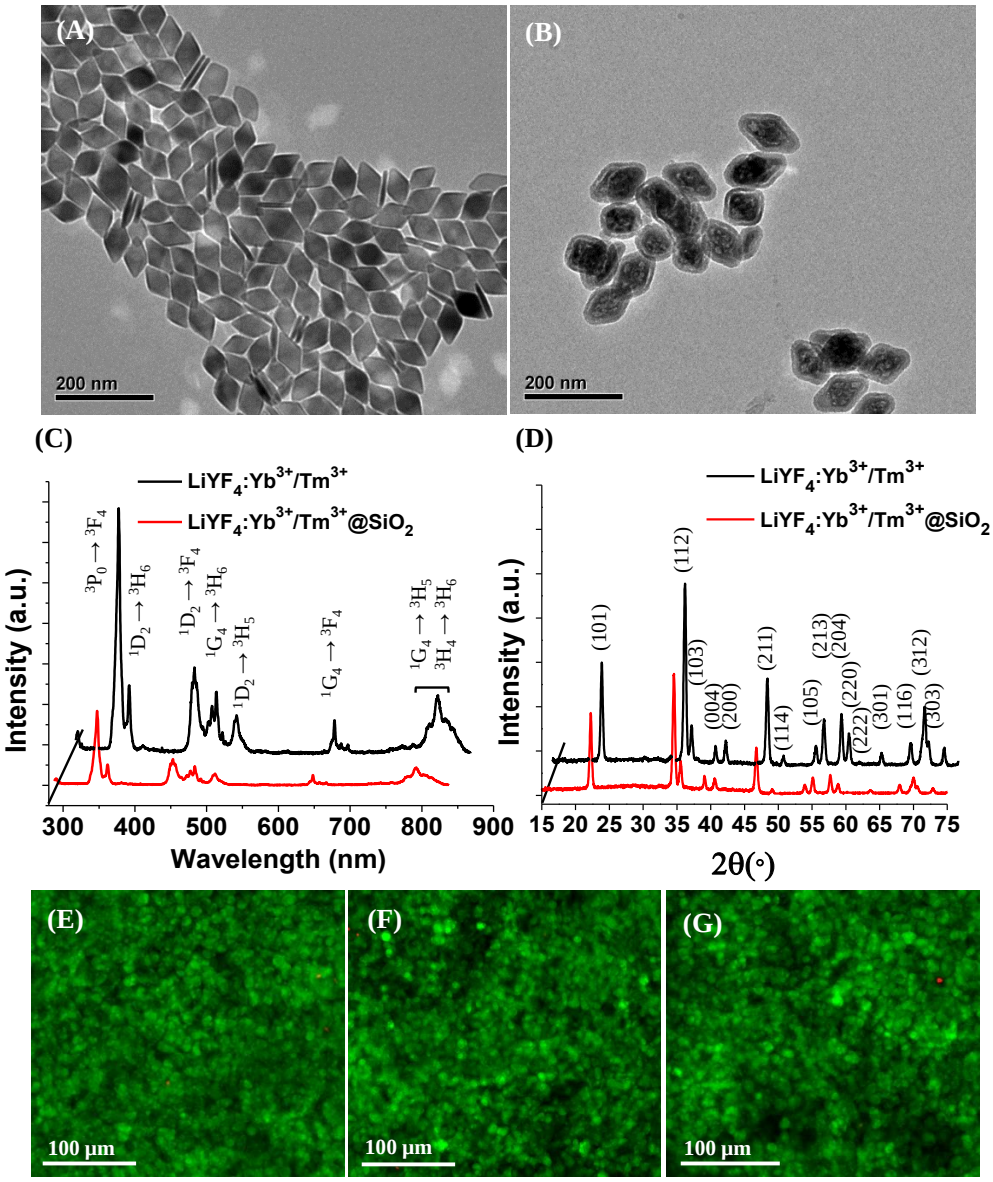


**Figure 2.** TEM images of (A) UCNPs and (B) UCNPs@$SiO_2$, showing homogenous UCNPs with narrow size distribution. (C) PL spectra of UCNPs (black line) and UCNPs@$SiO_2$ (red line). (D) X-ray diffraction patterns of UCNPs (black line) and UCNPs@$SiO_2$ (red line) with corresponding (*h k l*) values. Combined Live/Dead fluorescent images of chondrocytes cultured in DMEM-HG supplemented with (E) 0.05, (F) 0.2 and (G) 0.5 mg/ml of UCNPs@$SiO_2$.

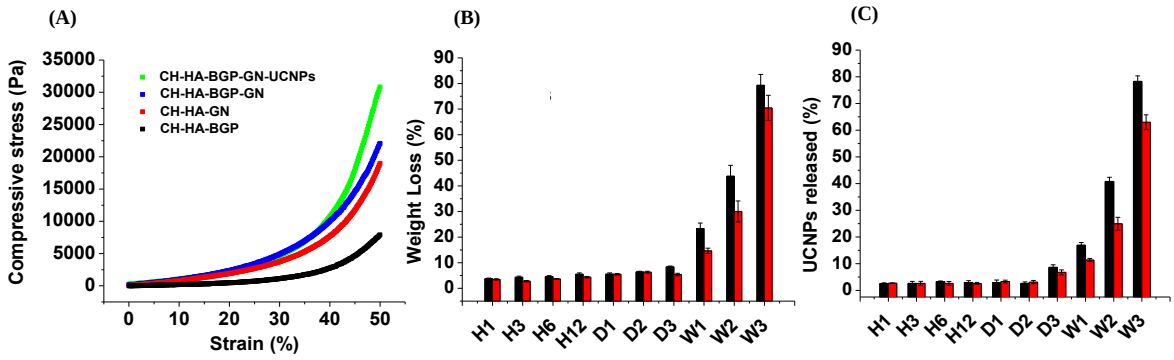


**Figure 3.** (A) Stress-strain curves for CH-HA gels crosslinked with BGP (black), GN (red), BGP-GN (blue) and BGP-GN with the addition 0.5mg/ml of UCNPs@$SiO_2$ (green). (B) Degradation rate of CH-HA-BGP-GN/UCNPs@$SiO_2$ gels and (C) release of UCNPs@$SiO_2$ in the presence PBS (red) and PBS-lysozyme (black) over a period of 3 weeks (H represents hours, D represents days and W represents weeks in figure B and C. Error bars in B and C represent standard deviation among three different batches N=3).

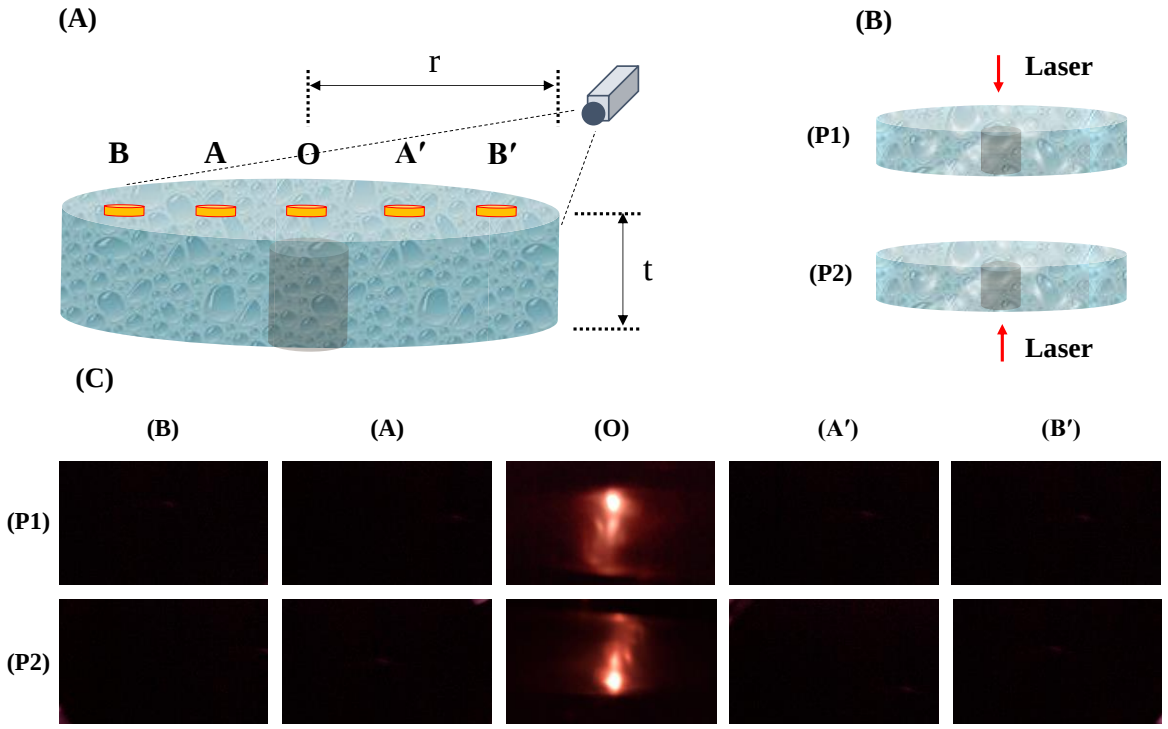


**Figure 4.** (A) Schematic showing the IVD and the location of the points irradiated by the laser. The IVD diameter (2r) is 26±2 mm and thickness (t) is 11 ± 1 mm. Spot O represents the center of the IVD, while spots A, A', B, and B' are located on the IVD diameter at a distance of 5 and 10 mm from the center. (B) Schematic showing the two configurations used to check the effect of laser positioning, either from the top (P1) or the bottom (P2) of the IVD. (C) NIR images of IVD injected with CH-HA-BGP-GN/UCNPs@$SiO_2$ gels on day zero, collected after irradiating with the laser at the locations O, A, B, A' and B' shown in panel A, in the configurations P1 and P2 shown in panel B. All NIR images are filtered through a band pass filter allowing only 775-825 nm light to pass through.

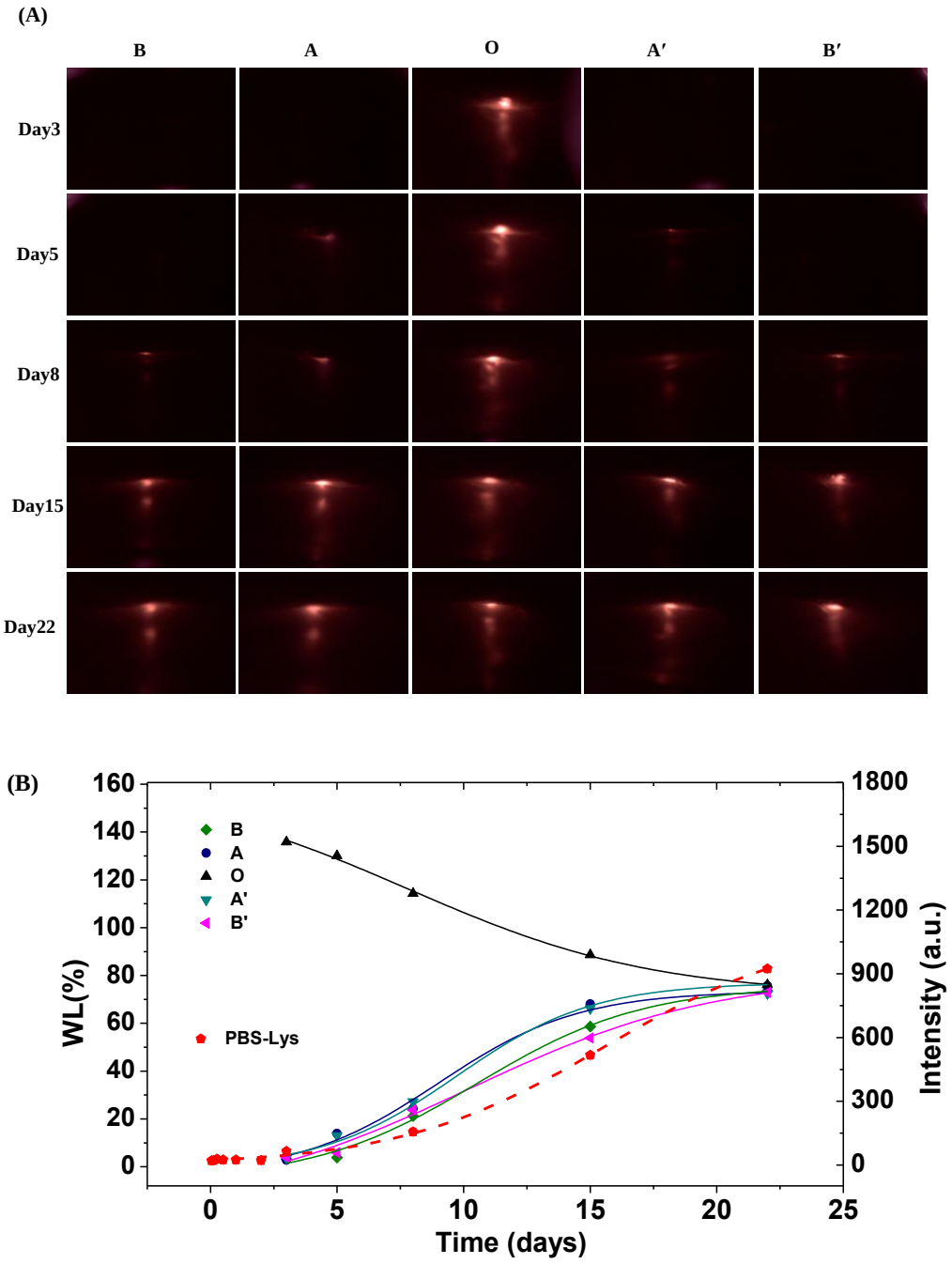


**Figure 5.** (A) NIR images of IVDs injected with CH-HA-BGP-GN/UCNPs@$SiO_2$, taken while shining with 975 nm light at the locations shown in Figure 4A over a period of 3 weeks, with the laser shining from the top of the IVD (configuration P1 in Figure 4B). All NIR images are filtered through a band pass filter allowing only 775-825 nm light to pass through. (B) Plots of PL intensity measured at $\lambda$ = 792 nm while shining the laser on positions O, A, A', B and B' on the IVD as a function of time. *In-vitro* UCNP release (dotted line) previously reported in Figure 3C is re-plotted for comparison.

**Table of contents entry only**

**Real-time, non-invasive monitoring of hydrogel degradation using $LiYF_4:Yb^{3+}/Tm^{3+}$ NIR-to-NIR upconverting nanoparticles**

$LiYF_4:Yb^{3+}/Tm^{3+}$ upconverting nanoparticles are used for real-time tracking of degradation of chitosan-hyaluronic acid gels in live intervertebral discs. The gels degrade over time and nanoparticles leach out, whose location is detected by NIR imaging and photoluminescence spectroscopy. The change in the intensity of upconverting nanoparticles is used to estimate the extent of gel degradation.

Ghulam Jalani, Rafik Naccache, Derek H Rosenzweig, Sophie Lerouge, Lisbet Haglund, Fiorenzo Vetrone* and Marta Cerruti*

**Keyword:** Non-invasive, upconverting nanoparticles, hydrogels, degradation